Atmospheric Environment 221 (2020) 117098

Contents lists available at ScienceDirect

Atmospheric Environment

journal homepage: http://www.elsevier.com/locate/atmosenv

Regional atmospheric pollutant transport mechanisms over the North China Plain driven by topography and planetary boundary layer processes

Jiannong Quan [a,*], Youjun Dou [a], Xiujuan Zhao [a,**], Quan Liu [b], Zhaobin Sun [a], Yubing Pan [a], Xingcan Jia [a], Zhigang Cheng [a], Pengkun Ma [a], Jie Su [a], Jinyuan Xin [c], Yangang Liu [d]

[a] Institute of Urban Meteorology, CMA, Beijing, China
[b] Beijing Key Laboratory of Cloud, Precipitation, and Atmospheric Water Resources, Beijing, China
[c] Institute of Atmospheric Physics, Chinese Academy of Sciences, Beijing, China
[d] Brookhaven National Laboratory, Upton, NY, USA

HIGHLIGHTS

- The mountain-induced vortex elevated surface pollutants to high layer.
- Pollutant in the EPL was transported downward to the surface through PBL process.
- Regional atmospheric pollutant transport mechanisms over NCP are suggested.

ARTICLE INFO

Keywords:
Vertical vortex
Elevated pollutant layer
PBL
Regional pollutant transport

ABSTRACT

Comprehensive measurements were conducted in winter 2018 and combined with RMPAS-Chem model simulations to analyze the regional transport mechanisms of atmospheric pollutants over the North China Plain. The instruments used consisted of four Vaisala CL51 ceilometers for planetary boundary layer (PBL) heights and aerosol backscatter profiles, two wind profilers, one radiosonde for the profiles of meteorological variables, and an instrumented King-Air 350 aircraft for the profiles of atmospheric pollutants and meteorological variables. Additionally, observations from Environmental Protection Bureau stations were also analyzed, including hourly concentrations of surface $PM_{2.5}$, SO_2, NO_2, CO, and O_3. The results suggest that regional atmospheric pollutant transport is driven by a combination of topography and PBL processes. First, a mountain-induced vertical vortex forms over downwind regions; this elevates ground pollutants to form an elevated pollutant layer (EPL) at an altitude of 1.4–1.7 km. The EPL is then transported to Beijing via an enhanced southerly wind. Finally, the pollutants in the EPL are transported downward to the surface through PBL processes.

1. Introduction

The North China Plain (NCP) has experienced heavy air pollution over the past two decades with particulate matter (PM) being one of the top pollutants (Che et al., 2007; Quan et al., 2011). PM, especially fine particulates ($PM_{2.5}$: PM with a radius ≤ 2.5 μm), can reach concentrations of several hundred micrograms per cubic meter in heavy haze events (Quan et al., 2014; Sun et al., 2014; Wang et al., 2014a), which is much higher than the value defined in the new National Ambient Air Quality Standards of China (75 μg m^{-3} for a 24 h average). Over the last decade, extensive efforts have been devoted to characterizing the sources and properties of $PM_{2.5}$ and haze pollution processes in the NCP (Cheng et al., 2016; Guo et al., 2014; Liu et al., 2018; Petäjä et al., 2016; Quan et al., 2017; Zhang et al., 2015, 2018). In general, high emissions of primary aerosols, gaseous precursors of secondary aerosols, and stagnant meteorological conditions have been considered the dominant factors driving the formation and evolution of haze pollution (Wang et al., 2014b; Guo et al., 2014; Zhang et al., 2015).

Beijing is located at the northern tip of the NCP and is bordered by mountains along its west, north, and northeast sides. Previous studies have indicated that the air pollution in Beijing is not only a local issue, but also a regional issue (An et al., 2007; Streets et al., 2007; Hua et al.,

* Corresponding author.
** Corresponding author.
E-mail addresses: jnquan@ium.cn (J. Quan), xjzhao@ium.cn (X. Zhao).

https://doi.org/10.1016/j.atmosenv.2019.117098
Received 26 April 2019; Received in revised form 28 October 2019; Accepted 30 October 2019
Available online 5 November 2019

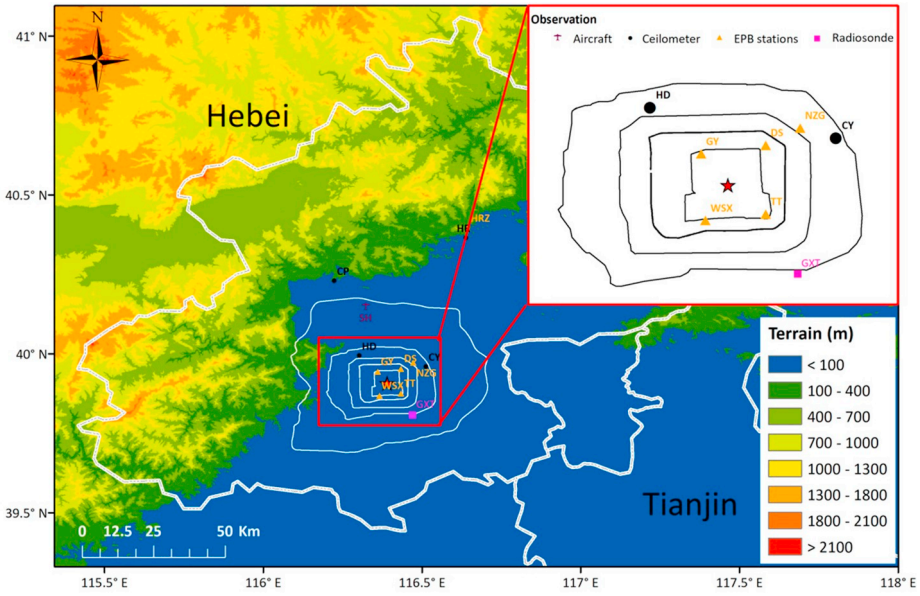

Fig. 1. Illustration of observation sites during the comprehensive measurements conducted in winter of 2018. The pentacle, triangle, circle, and square represent the locations of the center of Beijing city, ceilometer stations, EPB stations, and radiosonde station, respectively. The black lines in the top-right corner represent the second to fifth rings surrounding central Beijing and the central Changan street of Beijing city (straight line).

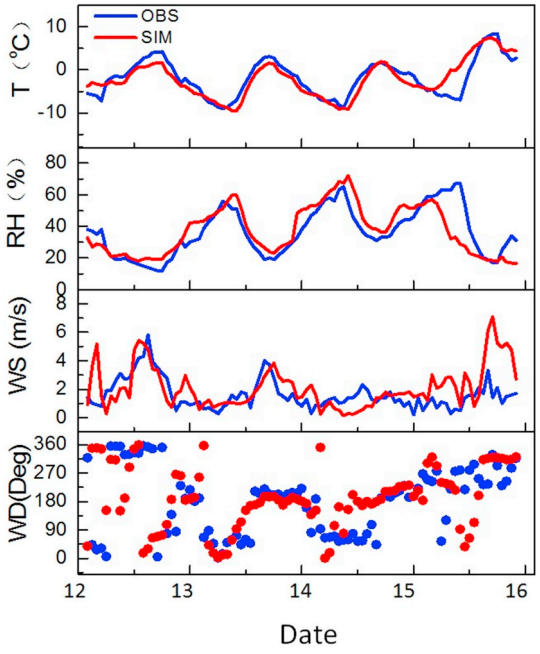

Fig. 2. Comparisons of meteorological elements between models and observations at the GXT station from the 13th to the 16th of December 2018, including temperature, RH, wind speed, and wind direction.

2016; Wang et al., 2016; Wu et al., 2017). For example, a community multi-scale air quality (CMAQ) model simulation by An et al. (2007) indicated that regional transport from the areas surrounding Beijing contributed 39% of $PM_{2.5}$, 30% of PM_{10}, and 18% of SO_2 to the city on average in a heavy pollution episode in spring of 2005. Similarly, a CMAQ model simulation of the Beijing region for July of 2001 reported by Streets et al. (2007) also indicated the regional transport of $PM_{2.5}$ and O_3 between Beijing and the NCP. In regional pollutant transport, topography is a non-negligible factor because it can influence the wind fields that drive pollutant transport. For example, Xu et al. (2015) suggested that the "harbor" effect of the westerlies in the eastern lee of the Tibetan Plateau may be an important factor influencing the occurrence of haze in eastern China. Similar phenomena were also observed in other regions with mountainous topography (Alizadeh-Choobari et al., 2016; Sabetghadam et al., 2018). A few studies have examined the potential influence of topography on regional pollutant transport over the NCP and found some intriguing results (Xu et al., 2015; Zhang et al., 2018). For example, Zhang et al. (2018) investigated the responses of surface winds to topographical changes. They found that if mountain heights decreased by 75%, Beijing and its surrounding areas would be controlled by northerly winds rather than southerly ones. Furthermore, topography also contributes to changes in vertical circulation (Wu et al., 2005; Sandu et al., 2019), which influences the vertical exchange of pollutants. Despite these studies and some general understanding of pollutant transport, the detailed mechanisms underlying the influence of topography on regional pollutant transport remain poorly understood.

Furthermore, vertical pollutant transport is strongly related to planetary boundary layer (PBL) structure. Inside the PBL, pollutants are vertically mixed by small eddy turbulences. However, there is generally a barrier (very low mixing rate) at the top of the PBL, which prevents the vertical transport of pollutants between the PBL and free troposphere (FT; Zhang et al., 2009; Quan et al., 2013). Regardless, aerosols can escape from the PBL to the FT through additional complex processes, such as frontal systems (dust storms), local circulation, and diurnal PBL variation, forming high aerosol concentrations in the FT. For example, in PBL development, turbulence weakens drastically after sunset and PBL height begins to decrease. In this process, aerosols in the upper PBL cannot return to the PBL with the decreasing of PBL height, instead forming a residual mixed layer. The wind speed in the FT is higher than that in the PBL, which enhances regional transport once aerosols are transported vertically into the FT. It is important to determine if regional pollutant transport mainly occurs inside or outside the PBL. Furthermore, if transport occurs outside the PBL, it is important to determine how FT pollutants are transported to the surface.

In this study, comprehensive measurements and model simulations were combined to analyze regional pollutant transport. The remainder of this paper is organized as follows. Section 2 describes the measurements and model simulations used in this study. Results and analyses are presented in Section 3. The analyses focus on (1) topography-induced vertical vortex and the formation of an elevated pollution layer (EPL), and (2) vertical pollutant transport through PBL processes. Section 4

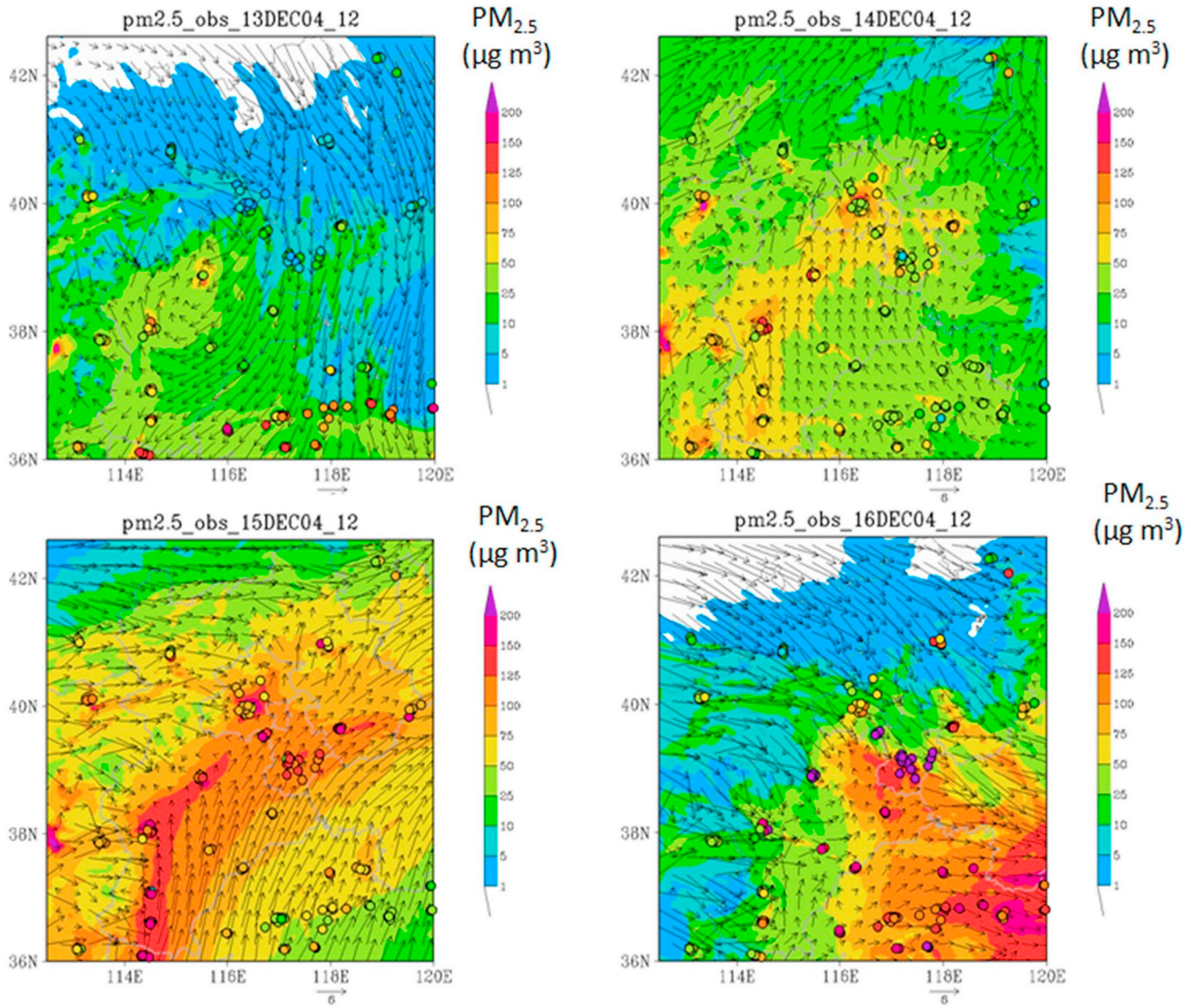

Fig. 3. Evaluation of models based on observations at 12:00 on the 13th, 14th, 15th, and 16th of December 2018. The dots represent observations from Chinese environmental monitoring stations (http://www.cnemc.cn/).

contains our concluding remarks.

2. Observations and methods

2.1. Observations

Comprehensive measurements were conducted in winter of 2018. The surface observation equipment used in this study consisted of four Vaisala CL51 ceilometers at Haidian (HD), Chaoyang (CY), Changping (CP), and Huairou (HR) for PBL heights and aerosol backscatter profiles, two wind profilers at HD and HR, and one radiosonde at the Guanxiangtai (GXT) meteorological station. The CL51 device utilizes the laser lidar technique (910 nm) to measure atmospheric aerosol backscatter profiles and has a detection range of 15.4 km. Its temporal and vertical resolutions are 6–120 s and 10 m, respectively. The radiosondes were launched twice per day at 08:00 and 20:00 BST (where BST = UTC + 8 h). Details regarding these instruments were provided by Liang et al., (2018). An aircraft (King-Air 350) was used to conduct the measurement of vertical aerosol profiles and meteorological variables. The typical aircraft speed was approximately 250 km h^{-1} and the ascent and descent rates during profiling were in the range of 2–5 m s^{-1}. A passive cavity aerosol spectrometer probe (PCASP, DMT Co., USA) was mounted on the aircraft wingtip to measure aerosol size distributions ranging from 0.1 to 3.0 μm at a frequency of 1 Hz. An integrated meteorological measurement system (Aimms-20, Advantech Research Inc.) was used to measure the aircraft location, temperature, relative humidity, barometric pressure, and wind speed. Additional details regarding the instrumentation and data processing are provided in the papers by Liu et al. (2019) and Quan et al. (2017). Before takeoff, all instruments were operated for 1–2 h to ensure they were working properly. As Shahe airport is not a commercial airport, there are only a few flights per day; therefore, the effects of aircraft emissions were minor in terms of the measured vertical distributions of aerosols. Additionally, observations from five Environmental Protection Bureau (EPB) stations in Beijing were analyzed. These data included the hourly concentrations of surface $PM_{2.5}$, SO_2, NO_2, CO, and O_3. The locations of the observation sites are presented in Fig. 1.

2.2. Models

The model used in this work was the RMPAS-Chem (Zhao et al.,

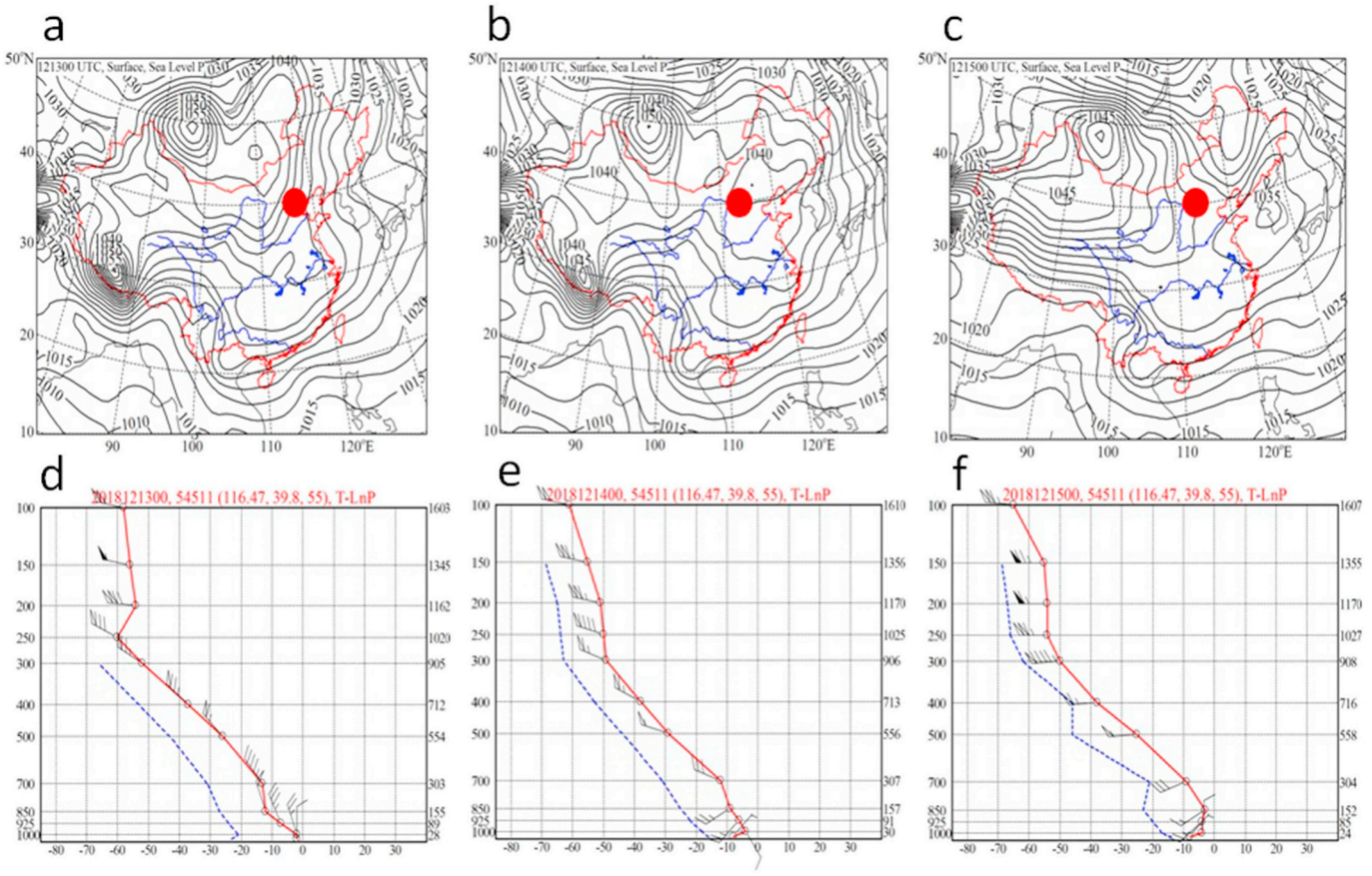

Fig. 4. Weather systems at 08:00 BST on the (a) 13th, (b) 14th, and (c) 15th of December 2018. The circles represents the location of Beijing city. Profiles of temperature (red line), dew point temperature (blue line), and wind over the Beijing GXT meteorological station at 08:00 on the (d) 13th, (e) 14th, and (f) 15th of December 2018. (For interpretation of the references to colour in this figure legend, the reader is referred to the Web version of this article.)

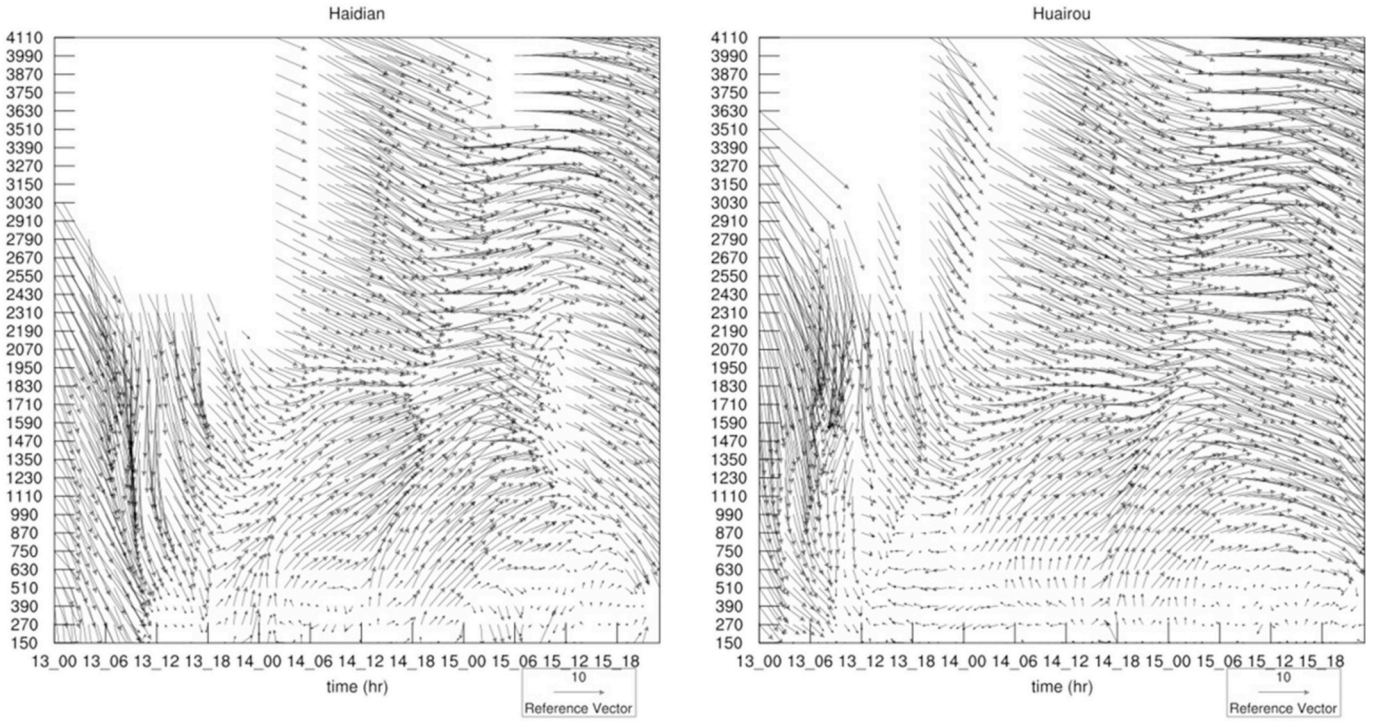

Fig. 5. Wind profiles (unit: m s^{-1}) at the HD (left) and HR (right) stations from the 13th to the 16th of December 2018.

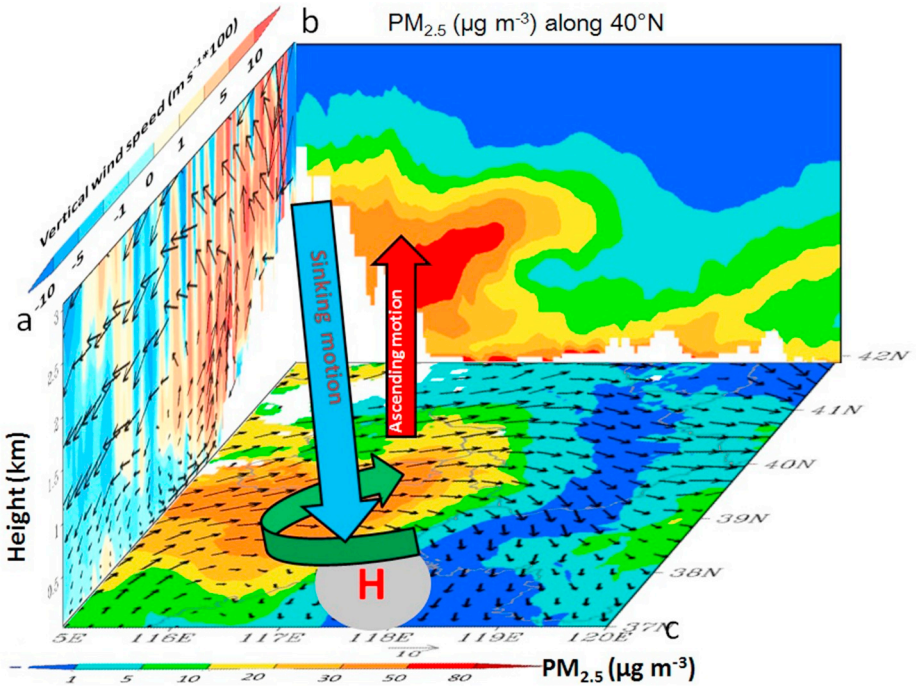

Fig. 6. Schematic diagram summarizing the formation of a topography-induced EPL over the NCP. Part (a) presents radial and vertical winds along the 116.64 °E line. The vertical winds have been multiplied by 100. The blue color represents sinking motion and the red color represents ascending motion. Part (b) presents the vertical $PM_{2.5}$ concentration along the 40 °N line. Part (c) presents the horizontal winds and $PM_{2.5}$ concentration at an altitude of 1500 m. The letter "H" in the base map represents an anomalous high-pressure system. (For interpretation of the references to colour in this figure legend, the reader is referred to the Web version of this article.)

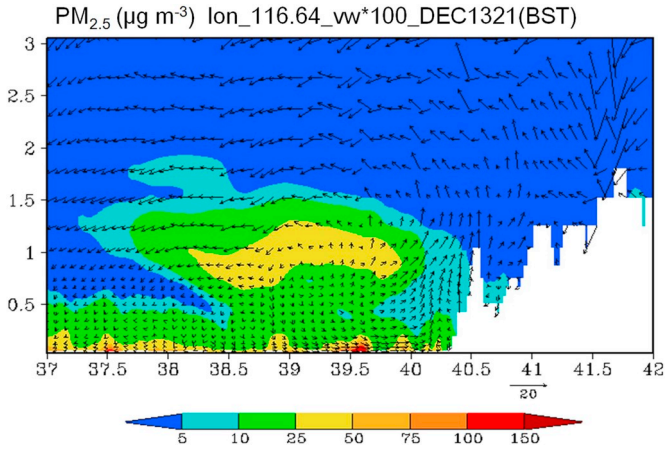

Fig. 7. Radial winds (unit: m s^{-1}) and $PM_{2.5}$ concentrations along the 116.64 °E line at 21:00 on December 13th, 2018 (same time as Fig. 4a). The vertical winds have been multiplied by 100.

2016, 2019; Zhang et al., 2018) model developed by the Institute of Urban Meteorology of the China Meteorological Administration. This model combines the rapid-refresh multi-scale analysis and prediction system - short term (RMAPS-ST) with weather research and forecasting (WRF)-Chem (version 3.3.1). RMAPS-ST is composed of a WRF-based regional numerical weather prediction system and WRF data assimilation system (Chen et al., 2011; Liang et al., 2018; Xie et al., 2019). Its physical parameterizations include the single-layer urban canopy model, Noah land surface, Yonsei University planetary boundary layer, Grell–Devenyi ensemble convection, Thompson cloud microphysics, and the rapid radiative transfer model for longwave and Goddard shortwave radiation (Chen and Dudhia, 2001; Hong and Kim, 2008; Grell and Devenyi, 2002; Thompson et al., 2008; Mlawer et al., 1997; Dudhia, 1989). The data assimilated in RMAPS-ST includes upper air, aircraft, surface, ground-based global positioning system zenith total delay, and radar observation data. In WRF-Chem, the carbon-based mechanism version Z is used, including comprehensive chemical reactions and alterable scenarios, in conjunction with the Model for Simulating Aerosol Interactions and Chemistry with four bin sizes (Zaveri and Peters, 1999; Zaveri et al., 2008). Anthropogenic precursor emission data were collected from the Multi-resolution Emission Inventory for China (2012) (http://www.meicmodel.org/) with a resolution of 0.1° × 0.1° and values extrapolated to 3 and 9 km grids. Meteorological ICs and BCs from the 9 km operational outputs of RMAPS-ST were directly applied to the 9 km WRF-Chem grid, then interpolated to the 3 km grid. The RMAPS-ST and RMAPS-Chem models provide daily meteorological and air pollution forecasting results for Beijing and the NCP (http://www.ium.cn/rmaps/st03/and http://www.ium.cn/rmaps/chem/), and have been evaluated against yearly observations (Liu and Chen, 2014; Zhao et al., 2016, 2019). The overall agreement between the simulations and measurements for both meteorological elements (Fig. 2) and $PM_{2.5}$ (Fig. 3) suggest that the models are capable of capturing the essential features of physical and chemical processes.

3. Results and analysis

3.1. Weather conditions

Beijing experienced an air pollution event from the 13th to the 16th of December in 2018. Fig. 4 presents the surface atmospheric circulations and radiosonde profiles of wind, temperature, and dew point temperature at the GXT meteorological station during this period. In the early stages (Dec. 13th), the Beijing region was controlled by a high-pressure system with two high-pressure centers located over the Tibetan plateau and Mongolia (Fig. 4a). Under these weather conditions, the Beijing region was influenced by a northwest wind (Fig. 4d). As the high-pressure system moved east (Fig. 4b and c), the northwest wind changed gradually into a south wind below the 850 hPa level (Fig. 4d and e). The wind profiles observed at the HD and HR stations clearly reveal that the wind direction in the lower layer (<1800 m) changed from northwest to southwest at 18:00 on Dec. 13th, whereas the higher level was still controlled by the northwest wind (Fig. 5).

3.2. Topography-induced EPL

Beijing is bordered by mountains along the west, north, and

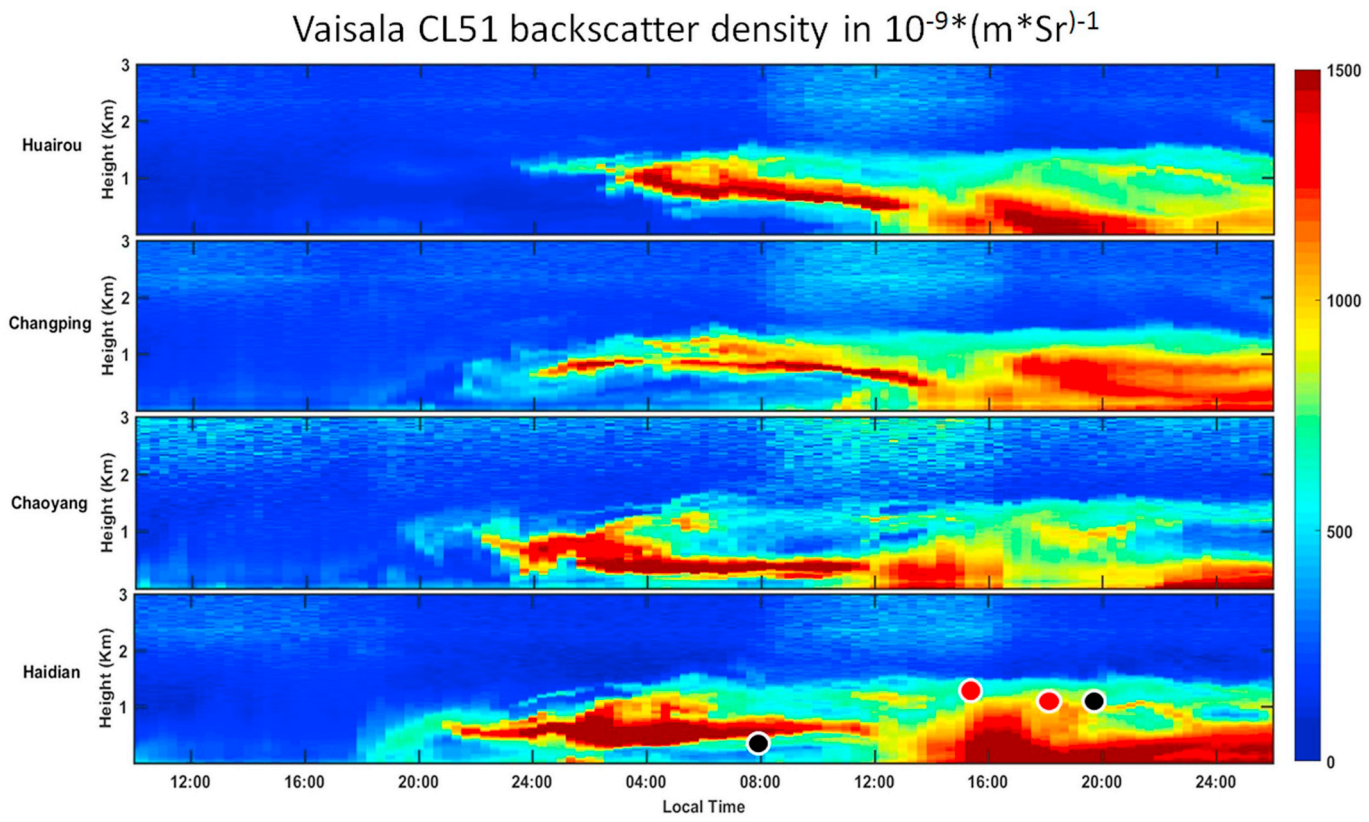

Fig. 8. Aerosol backscatter coefficients at four stations: (a) HR, (b) CP, (c) CY, and (d) HD. The dots on the bottom represent the PBL heights calculated from sounding (black) and aircraft data (red). (For interpretation of the references to colour in this figure legend, the reader is referred to the Web version of this article.)

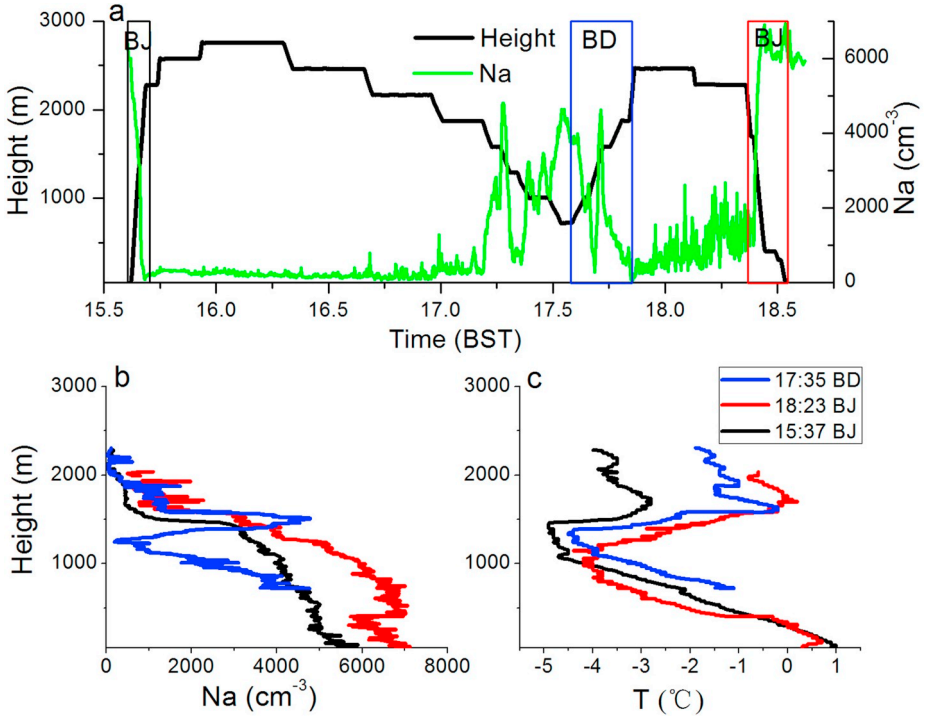

Fig. 9. (a) Flight height (black line) and aerosol number concentration (Na, green line) observed by the PCASP, (b) vertical profiles of aerosol particles, and (c) temperature over Baoding (BD, blue line) and Beijing (BJ) during takeoff (black line) and landing (red line). (For interpretation of the references to colour in this figure legend, the reader is referred to the Web version of this article.)

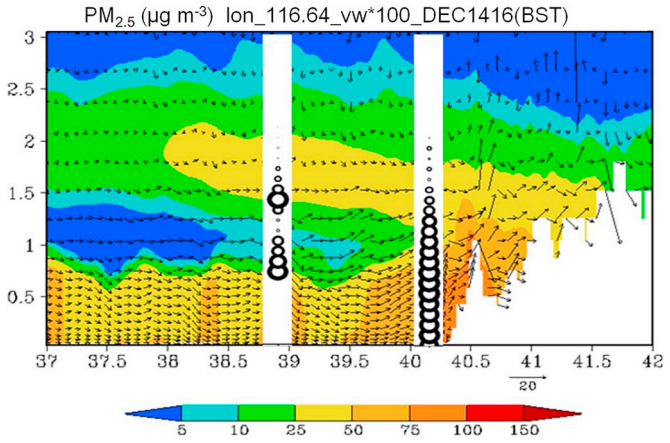

Fig. 10. Radial winds (unit m s^{-1}) and $PM_{2.5}$ concentrations along the 116.64 °E line at 16:00 on December 14th, 2018. The vertical winds have been multiplied by 100. The circles represent aerosol number concentrations observed by the aircraft, where the sizes of the circles correspond to concentrations.

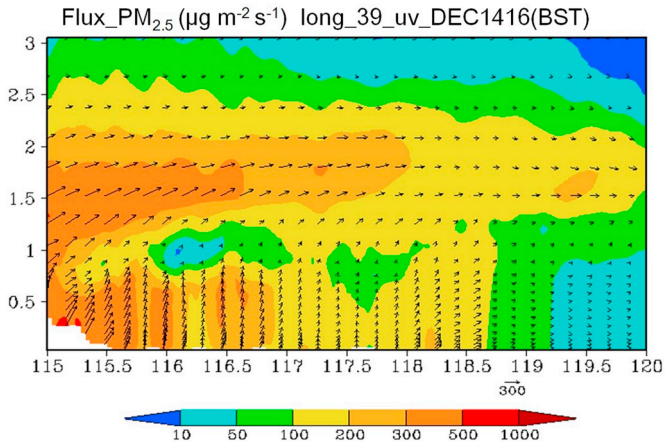

Fig. 11. Transport flux of $PM_{2.5}$ (μg $m^{-2} s^{-1}$) along the 39 °N line at 16:00 on December 14th, 2018. The colors represent flux and the arrows represent directions in the u-v space. (For interpretation of the references to colour in this figure legend, the reader is referred to the Web version of this article.)

northeast sides, with altitudes exceeding 1000 m (Fig. 1). Based on the blocking role of such topography, the north wind over downwind regions of the mountains was weakened (Zhang et al., 2018). Furthermore, a vertical vortex in the lower troposphere was induced over downwind regions of the mountains (Fig. 6). A sinking motion occurred in regions with latitudes between 37 °N and 38 °N, whereas ascending motion occurred in regions near the mountains with latitudes between 39 °N and 41 °N. Zhang et al. (2018) investigated the responses of surface winds to topographical changes. Their work indicated that Beijing and the surrounding area would be controlled by north wind, rather than south wind, if the mountain height decreased by 75%, which clearly demonstrates the role of the mountains in shaping local vertical vortices.

The mountain-induced vertical vortex elevated ground pollutants to higher layers. This point was supported by our model results, which revealed high $PM_{2.5}$ centers in regions with altitudes in the range of 1.0–1.5 km (Figs. 6b and 7), which are consistent with the center of the vertical vortex. Under the collective influence of the vertical vortex and eastward movement of the high pressure system, the wind direction in the lower layer gradually shifted from north to south (Fig. 5). Therefore, the EPL was transported north. These findings were substantiated by ceilometer observations. A clear EPL was observed over Beijing on the

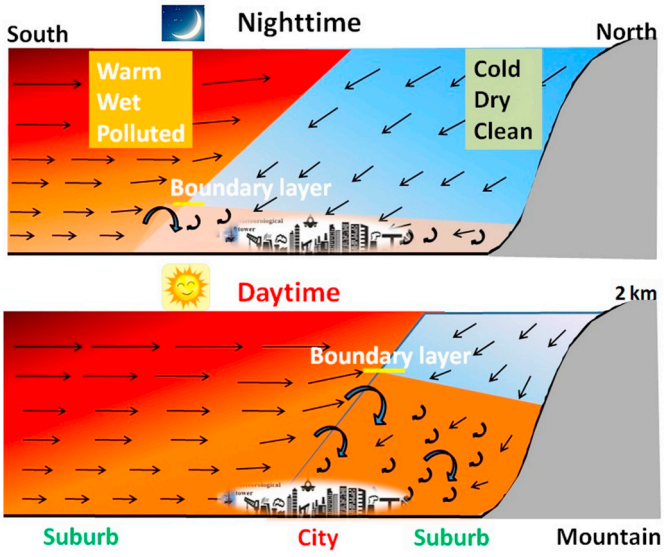

Fig. 12. Schematic diagram summarizing downward pollutant transport via PBL processes. At night, the downward transport of pollutants in the EPL is weak based on the low PBL height. However, the PBL height increases during the day. Therefore, the EPL moves from outside the PBL to inside the PBL, which accelerates downward pollutant transport.

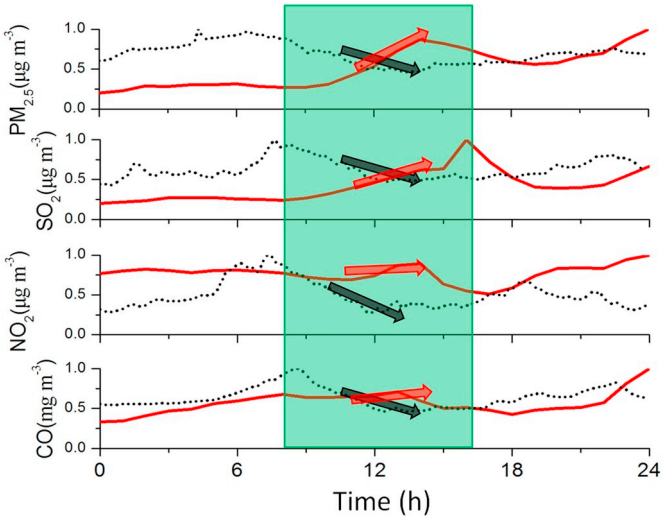

Fig. 13. Average diurnal variations of pollutants at five urban EPB stations on December 14th, 2019 (red lines). The dotted lines represent typical diurnal pollutant variations, which are dominantly controlled by PBL processes (Quan et al., 2013). (For interpretation of the references to colour in this figure legend, the reader is referred to the Web version of this article.)

night of Dec. 13th and morning of Dec. 14th. Furthermore, among the four ceilometers stations (Fig. 8), the EPL first appeared at the southern stations (20:00 on Dec. 13th at HD, CY), then the northern stations (CP, HR), indicating that the EPL was transported from south to north.

Aircraft measurements were also conducted on Dec. 14th of 2018. The King-Air 350 aircraft took off and climbed to approximately 2700 m over the Shahe airport, which is located 35 km north of Beijing city (Fig. 1). The aircraft then flew southwest for approximately 150 km to reach the Baoding area, where it collected vertical profiles in step levels of 300 m (from 2700 to 600 m). Finally, the aircraft flew back to the Shahe airport (Fig. 9). The vertical profiles of aerosol concentrations over Baoding exhibited a distinct EPL between 1400 and 1700 m at 17:35 on the afternoon of Dec. 14th, with a maximum aerosol number

concentration (N_a) of 5000 cm^{-3} (Fig. 9). Below this layer, a clean layer can be observed between 1100 and 1300 m with a N_a value less than 1000 cm^{-3}. The existence of an EPL over Baoding was further corroborated by the model results (Fig. 10). Based on the enhancement of the south wind, the EPL was transported north to Beijing. To analyze the contributions of the EPL to regional aerosol transport quantitatively, horizontal transport flux was calculated based on the $PM_{2.5}$ concentration and wind (Fig. 11). The results clearly reveal that were two layers with high $PM_{2.5}$ transport flux: one in the PBL and the other in the EPL. These results collectively suggest that the EPL between 1.0 and 1.5 km over Beijing was horizontally transported from upwind regions.

3.3. Downward transport

As shown in Fig. 8, an EPL was present over Beijing on the evening of Dec. 13th and morning of Dec. 14th but disappeared near 13:00 on the afternoon of Dec. 14th. Therefore, the aerosol concentration in the lower layer increased significantly on the afternoon of Dec. 14th. This prompted us to examine two questions. First, was the aerosol enhancement in the low layer related to the EPL? Second, if it was related, what was the main mechanism and why did it occur in the afternoon, rather than the evening? To answer these questions, we first analyzed the PBL, which is the lowest layer in the troposphere, where wind is influenced by friction. Surface friction causes turbulent eddies and chaotic wind patterns to develop. As a result, wind is turbulent and gusty within the PBL. In this study, PBL height was identified as the altitude at which there was an inversion or abrupt and significant change in the dew point temperature (Wilczak et al., 1996; Quan et al., 2013, 2017), which is calculated from aircraft/sounding measurements of temperature and relative humidity. The PBL height was low at night and early in the morning (e.g., 510 m at 08:00 in the morning of Dec. 14th). The height increased with an increase in solar radiation and reached a maximum value in the afternoon. The PBL height was 1650 m at 15:35 in the afternoon of Dec. 14th (Fig. 8). There typically is a barrier (very low mixing rate) at the top of the PBL that prevents the vertical transportation of pollutants between the PBL and FT (Zhang et al., 2009; Quan et al., 2013). At night and early in the morning, PBL height is low and the EPL is located above the PBL, so downward pollutant transport is limited. Based on the continued development of the PBL, the EPL moved from outside the PBL in the morning to inside the PBL in the afternoon (Fig. 8), which enhanced the vertical mixing of aerosols inside the PBL. Therefore, aerosols in the EPL were transported downward with an increase in PBL height in the afternoon. The processes described above are summarized in Fig. 12. The variations in ground pollutants substantiate these analyses (Fig. 13). When ground pollutants are dominantly affected by PBL processes, their concentrations typically decrease in the morning and reach minimum values in the afternoon based on the increased PBL height (dotted line in Fig. 13). In contrast, the concentrations of pollutants increased significantly in the afternoon of Dec. 14th, even though the PBL height also increased during this period (Fig. 8). The concentration of pollutants during this period should decrease, rather than increase, if there is no regional pollutant transport. Therefore, the increase in pollutants in the afternoon of Dec. 14th was primarily caused by the transport process.

4. Summary and discussion

In this study, comprehensive measurements were conducted in winter of 2018 and combined with RMPAS-Chem model simulations to analyze the regional transport mechanisms of atmospheric pollutants over the NCP. Based on the comprehensive measurements and model simulations, we determined that regional atmospheric pollutant transport is driven collectively by topography and PBL processes. Our main findings can be summarized as follows.

(1) Based on the blocking role of mountains, a vertical vortex in the lower troposphere was induced over downwind regions. This mountain-induced vortex elevated ground pollutants to higher layers and formed an EPL in the altitude range of 1.4–1.7 km. The existence of the EPL was confirmed based on the observations of ceilometers, aircraft measurements, and model simulations.
(2) The EPL was transported north to Beijing by an enhanced south wind. The pollutants in the EPL were eventually transported down to the surface through PBL processes. At night and early in the morning, the PBL height was low and the EPL was located above the PBL. The stable PBL prevented the downward transport of pollutants. In the afternoon, the EPL was located inside PBL based on its continued development, which helped transport aerosols in the EPL down to the surface. As a result, the surface aerosol concentration increased.
(3) It should be noted that only one pollution episode was analyzed in this study. Although the model simulations provided results consistent with the observations and substantiated our observational analysis, additional measurements should be conducted in the future. Additionally, it is noteworthy that this study was based on data collected in the NCP. Whether or not our findings can be generalized to other regions warrants further investigation.

Declaration of competing interest

The authors declare that they have no known competing financial interests or personal relationships that could have appeared to influence the work reported in this paper.

Acknowledgments

This research was supported by the National Key R&D Program of China (2017YFC0209604, 2018YFF0300101), Beijing Natural Science Foundation (8161004), and Beijing Major Science and Technology Project (Z181100005418014). Y. L. is supported by the Laboratory of Directed Research and Development program and the US Department of Energy's Atmospheric System Research program.

Appendix A. Supplementary data

Supplementary data to this article can be found online at https://doi.org/10.1016/j.atmosenv.2019.117098.

References

Alizadeh-Choobari, O., Bidokhti, A.A., Ghafarian, P., Najafi, M.S., 2016. Temporal and spatial variations of particulate matter and gaseous pollutants in the urban area of Tehran. Atmos. Environ. 141, 443–453.
An, X., Zhu, T., Wang, Z., Li, C., Wang, Y., 2007. A modeling analysis of a heavy air pollution episode occurred in Beijing. Atmos. Chem. Phys. 7, 3103–3114.
Che, H., Zhang, X., Yang, L., Zhou, Z., Qu, J.J., 2007. Horizontal visibility trends in China 1981-2005. Geophys. Res. Lett. 34, 497–507.
Chen, F., Dudhia, J., 2001. Coupling an advanced land-surface hydrology model with the Penn State-NCAR MM5 modeling syste. Part I: model implementation and sensitivity. Mon. Weather Rev. 129, 569–585.
Chen, M., Fan, S.Y., Zheng, Z.F., Zhong, J.Q., 2011. The performance of the proximity sounding based on the BJ-RUC system and its preliminary implementation in the convective potential forecast (in Chinese). Acta Meteorol. Sin. 69, 181–194.
Cheng, Y.F., Zheng, G.J., Wei, C., Mu, Q., Zheng, B., Wang, Z.B., Gao, M., Zhang, Q., He, K.B., Carmichael, G., Pöschl, U., Su, H., 2016. Reactive nitrogen chemistry in aerosol water as a source of sulfate during haze events in China. Sci. Adv. 2, e1601530.
Dudhia, J., 1989. Numerical study of convection observed during the Winter Monsoon Experiment using a mesoscale two dimensional model. J. Atmos. Sci. 46 (20), 3077–3107.
Grell, G.A., Devenyi, D., 2002. A generalized approach to parameterizing convection combining ensemble and data assimilation techniques. Geophys. Res. Lett. 29 (14), 1693.
Guo, S., Hu, M., Zamora, M.L., Peng, J.F., Shang, D.J., Zheng, J., Du, Z.F., Wu, Z.J., Shao, M., Zeng, L.M., Molina, M.J., Zhang, R.Y., 2014. Elucidating severe urban haze formation in China. Proc. Natl. Acad. Sci. U.S.A. 111, 17373–17378.

Hong, S.-Y., Kim, S.-W., 2008. Stable boundary layer mixing in a vertical diffusion scheme. Proc. Ninth Annual WRF User's Workshop. National Center for Atmospheric Research, Boulder, CO, 3.3. [Available online at: http://www.mmm.ucar.edu/wrf/users/workshops/WS2008/abstracts/3-03.pdf.

Hua, Y., Wang, S.X., Wang, J.D., Jiang, J.K., Zhang, T.S., Song, Y., Kang, L., Zhou, W., Cai, R.L., Wu, D., Fan, S.W., Wang, T., Tang, X.Q., Wei, Q., Sun, F., Xiao, Z.M., 2016. Investigating the impact of regional transport on PM2.5 formation using vertical observation during APEC 2014 Summit in Beijing. Atmos. Chem. Phys. 16, 15451–15460.

Liang, X., Miao, S., Li, J., BornStein, R., Zhang, X., Gao, Y., Chen, F., Cao, X., Cheng, Z., Clements, C., Dabberdt, W., Ding, A., Ding, D., Dou, J.J., Dou, J.X., Dou, Y., Grimmond, C.S.B., Gonzalez-Cruz, J.E., He, J., Huang, M., Huang, X., Ju, S., Li, Q., Niyogi, D., Quan, J., Sun, J., Sun, J.Z., Yu, M., Zhang, J., Zhang, Y., Zhao, X., Zheng, Z., Zhou, M., 2018. SURF: understanding and predicting urban convection and haze. Bull. Am. Meteorol. Soc. https://doi.org/10.1175/BAMS-D-16-0178.1.

Liu, M., Chen, M., 2014. Evaluation of BJ-RUC system for the forecast quality of planetary boundary layer in Beijing area (in Chinese). J. Appl. Meteorol. Sci. 25, 212–221.

Liu, Q., Jia, X.C., Quan, J.N., Li, J., Li, X., Wu, Y., Chen, D., Wang, Z., Liu, Y., 2018. New positive feedback mechanism between boundary layer meteorology and secondary aerosol formation during severe haze events. Sci. Rep. 8, 6095.

Liu, Q., Quan, J.N., Jia, X.C., Sun, Z., Li, X., Gao, Y., Liu, Y., 2019. Vertical profiles of aerosol composition over Beijing, China: analysis of in-situ aircraft measurements. J. Atmos. Sci. https://doi.org/10.1175/JAS-D-18-0157.1.

Mlawer, E.J., Taubman, S.J., Brown, P.D., Iacono, M.J., Clough, S.A., 1997. RRTM, a validated correlated-K model for the longwave. J. Geophys. Res. 102 (D14), 16663–16682.

Petäjä, T., Järvi, L., Kerminen, V.-M., Ding, A.J., Sun, J.N., Nie, W., Kujansuu, J., Virkkula, A., Yang, X.-Q., Fu, C.B., Zilitinkevich, S., Kulmala, M., 2016. Enhanced air pollution via aerosol boundary layer feedback in China. Sci. Rep. 6, 18998.

Quan, J.N., Zhang, Q., He, H., Liu, J., 2011. Analysis of the formation of fog and haze in North China Plain (NCP). Atmos. Chem. Phys. 11, 11911–11937.

Quan, J.N., Gao, Y., Zhang, Q., Tie, X., Cao, J., Han, S., Meng, J., Chen, P., Zhao, D., 2013. Evolution of planetary boundary layer under different weather conditions, and its impact on aerosol concentrations. Particuology 11, 34–40.

Quan, J.N., Tie, X., Zhang, Q., Liu, Q., Li, X., Gao, Y., Zhao, D., 2014. Characteristics of heavy aerosol pollution during the 2012-2013 winter in Beijing, China. Atmos. Environ. Times 88, 83–89.

Quan, J.N., Liu, Y., Liu, Q., Jia, X., Li, X., Gao, Y., Ding, D., Li, J., Wang, Z., 2017. Anthropogenic pollution elevates the peak height of new particle formation from planetary boundary layer to lower free troposphere. Geophys. Res. Lett. 44, 7537–7543.

Sabetghadam, S., Khoshsima, M., Alizadeh-Choobari, O., 2018. Spatial and temporal variations of satellite-based aerosol optical depth over Iran in Southwest Asia: identification of a regional aerosol hot spot. Atmos. Pollut. Res. 9, 849–856.

Sandu, I., van Niekerk, A., Shepherd, T.G., Vosper, S.B., Zadra, A., Bacmeister, J., Beljaars, A., Brown, A.R., Dörnbrack, A., McFarlane, N., Pithan, F., Svensson, G., 2019. Impacts of orography on large-scale atmospheric circulation. npj Clim. Atmos. Sci. 2, 10. https://doi.org/10.1038/s41612-019-0065-9.

Streets, D.G., Fu, J.S., Jang, C.J., Hao, J., He, K., Tang, X., Zhang, Y., Wang, Z., Li, Z., Zhang, Q., Wang, L., Wang, B., Yu, C., 2007. Air quality during the 2008 Beijing Olympic Games. Atmos. Environ. 41, 480–492.

Sun, Y., Jiang, Q., Wang, Z., Fu, P., Li, J., Yang, T., Yin, Y., 2014. Investigation of the sources and evolution processes of severe haze pollution in Beijing in January 2013. J. Geophys. Res. 119, 2014JD021641.

Thompson, G., Field, P.R., Rasmussen, R.M., Hall, W.D., 2008. Explicit forecasts of winter precipitation using an im-proved bulk microphysics scheme. Part II: implementation of a new snow parameterization. Mon. Weather Rev. 136, 5095–5115.

Wang, Q., Huang, R., Cao, J., Tie, X., Shen, Z., Zhao, S., Han, Y., Li, G., Li, Z., Ni, H., Zhou, Y., Wang, M., Chen, Y., Su, X., 2016. Contribution of regional transport to the black carbon aerosol during winter haze period in Beijing. Atmos. Environ. 132, 11–18.

Wang, Y.S., Yao, L., Wang, L., Liu, Z., Ji, D., Tang, G., Zhang, J., Sun, Y., Hu, B., Xin, J., 2014. Mechanism for the formation of the January 2013 heavy haze pollution episode over central and eastern China. Sci. China Earth Sci. 57, 14–25.

Wang, J., Wang, S., Jiang, J., Ding, A., Zheng, M., Zhao, B., Wong, D.C., Zhou, W., Zheng, G., Wang, L., Pleim, J.E., Hao, J., 2014. Impact of aerosol–meteorology interactions on fine particle pollution during China's severe haze episode in January 2013. Environ. Res. Lett. 9, 094002.

Wilczak, J.M., Gossard, E.E., Neff, W.D., Eberhard, W.L., 1996. Ground-based remote sensing of the atmospheric boundary layer: 25 years of progress. Boundary-Layer Meteorol. 78, 321–349.

Wu, G.X., Wang, J., Liu, X., Liu, Y.M., 2005. Numerical modeling of the influence of Eurasian orography on the atmospheric circulation in different seasons. Acta Meteorol. Sin. 63, 603–612.

Wu, J., Li, G., Cao, J., Bei, N., Wang, Y., Feng, T., Huang, R., Liu, S., Zhang, Q., Tie, X., 2017. Contributions of trans-boundary transport to summertime air quality in Beijing, China. Atmos. Chem. Phys. 17, 2035–2051.

Xie, Y.H., Fan, S.Y., Chen, M., Shi, J.C., Zhong, J.Q., Zhang, X.Y., 2019. An assessment of satellite radiance data assimilation in RMAPS. Remote Sens. 11, 54. https://doi.org/10.3390/rs11010054.

Xu, X.D., Wang, Y., Zhao, T., Cheng, X., Meng, Y., Ding, G., 2015. Harbor" effect of large topography on the haze distribution in eastern China and its climate modulation on decadal variations in haze China. Chin. Sci. Bull. 60, 1132–1143.

Zaveri, R.A., Peters, L.K., 1999. A new lumped structure photochemical mechanism for large-scale applications. J. Geophys. Res. 104, 30387–30415.

Zaveri, R.A., Easter, R.C., Fast, J.D., Peters, L.K., 2008. Model for simulating aerosol interactions and chemistry (MOSAIC). J. Geophys. Res. 113, D13204.

Zhang, Q., Ma, X.C., Tie, X., Huang, M., Zhao, C., 2009. Vertical distributions of aerosols under different weather conditions: analysis of in-situ aircraft measurements in Beijing, China. Atmos. Environ. Times 9, 4621–4638.

Zhang, Q., Quan, J., Tie, X., Li, X., Liu, Q., Gao, Y., Zhao, D., 2015. Effects of meteorology and secondary particle formation on visibility during heavy haze events in Beijing, China. Sci. Total Environ. 502, 578–584.

Zhang, Z.Y., Xu, X., Qiao, L., Gong, D., Kim, S.-J., Wang, Y., Mao, R., 2018. Numerical simulations of the effects of regional topography on haze pollution in Beijing. Sci. Rep. 8, 5504.

Zhao, X.J., Xu, J., Zhang, Z.Y., Zhang, X.L., Fan, S.Y., Su, J., 2016. Beijing regional environmental meteorology prediction system and its performance test of PM2.5 concentration. J. Appl. Meteorol. Sci. 27, 160–272 (in Chinese).

Zhao, X.J., Li, Z.M., Xu, J., 2019. Modification and performance tests of visibility parameterizations for haze days. Environ. Sci. 40 (4), 1688–1696 (in Chinese).